CONDUCTION HEAT TRANSFER THROUGH SOLID IN POROUS MATERIALS: A COMPARATIVE STUDY BY FINITE-ELEMENT SIMULATIONS AND EFFECTIVE MEDIUM APPROXIMATIONS

Amit Rai,¹ Tianli Feng,¹ Daniel Howard,¹ Diana Hun,¹ Mingkan Zhang,¹ Hongyu Zhou,² & Som S. Shrestha^{1,*}

Original Manuscript Submitted: 7/27/2020; Final Draft Received: 4/12/2021

The development of insulation materials with low effective thermal conductivity is essential for energy savings in various applications, including buildings, food services, pipe insulation, and refrigeration. Such materials can be developed by using micro- or nanoporous structures, as well as low—thermal conductivity gases and/or reduced pressure. A variety of effective medium approximation (EMA) models have been developed to study thermal transport through solid in porous structures. However, in many cases, the impacts of porosity on solid conduction are not well predicted by EMA models because of the assumptions made for simplification. Furthermore, the results can vary by a factor of up to 1.5, depending on the morphology of the pores. Hence, proper guidance is needed to choose the appropriate EMA model for a given morphology. This work presents a finite element method study using COMSOL Multiphysics software for various geometries, including hollow cubes, overlapping hollow spheres (normally stacked and tightly packed), and Voronoi structures, and compares the results to those obtained from various EMA models. Simulation results for the hollow cubes and Voronoi structures matched well with the Maxwell-Eucken and Russell model. The results for hollow spheres closely matched the Bauer model and the Glicksman model with fitting parameters. This work provides guidance on analyzing and designing insulation materials for energy savings in the future.

KEY WORDS: conduction heat transfer in porous materials, low thermal conductivity, effective medium approximations, finite element method

1. INTRODUCTION

Insulation materials play a significant role in energy savings. Hence, they are of great importance in applications such as buildings (Reimi et al., 2009; Jelle et al., 2010), the food and dairy industries (Deshmukh et al., 2017), pipe insulation, (Cai et al., 2014), refrigeration (Kayfeci and Keçebaş, 2013), and others. Heat transfer through porous materials can be modified in various ways to reduce the materials' effective thermal conductivity (ETC), such as creating different porous structures, reducing pore sizes, increasing porosity, and forming composites. The precise analysis and prediction of the thermal behaviors of such materials are sometimes mathematically and computationally challenging. Therefore, various models have been developed that can approximately describe useful parameters and properties of such materials based on the properties and the relative volume fractions of its constituents. Such approximations are known as effective medium approximation (EMA) models (Wang et al., 2008; Wang and Pan, 2008).

¹Energy and Transportation Science Division, Oak Ridge National Laboratory, Oak Ridge, TN, 37831, USA

²Department of Civil and Environmental Engineering, The University of Tennessee, Knoxville, TN, 37996, USA

^{*}Address all correspondence to: Som S. Shrestha, Energy and Transportation Science Division, Oak Ridge National Laboratory, Oak Ridge, Tennessee, 37831, USA; Tel.: +1 865 241 8772; Fax: +1 865 574 9354, E-mail: shresthass@ornl.gov

Low-thermal conductivity insulation materials can be developed by using micro- or nanoporous structures, as well as low-thermal conductivity gases or reduced pressure, to reduce heat transfer through the solid and gas components. In such materials, the pores are generally < 4 mm in diameter (on the order of micrometers and nanometers), causing complete suppression of convective heat transfer and making essentially no contribution to thermal conductivity (Hrubesh and Pekala, 1994; Hu et al., 2018). Thus, their total heat transfer is a combination of conduction and radiation. The conduction heat transfer mode is further divided into solid conduction and gaseous conduction (He and Xie, 2015). For most conventional insulation materials, the contribution from gas conduction is higher than that from solid conduction. However, in some cases, such as vacuum insulation panels, solid conduction is important (Baetens et al., 2010).

A variety of theoretical models have been developed to determine the effective thermal properties of composites and porous insulation materials. The geometry/morphology (shape and size) is one of the critical factors that can affect the effective thermal properties of such materials. However, to simplify the heat transfer analysis, most EMA models mainly focus on the composition of materials (and their relative volume fractions) and consider the internal geometry or microstructures to have simple geometrical arrangements. Because of their predictive power, easiness of calculation, and reasonable accuracy for certain cases (where microstructures can be simplified), such theoretical models are still preferred (Walser, 2009; Wang et al., 2008; Wang and Pan, 2008; Russell, 1935; Bauer, 1993). Shrestha et al. (2019) reviewed the models used for determining the ETC of a variety of insulation materials and enumerated the aspects that were not incorporated by those models. Maxwell (1904) developed a model to calculate the ETC of randomly distributed spheres in a continuous medium, which provided better results for low filler concentrations. Variations of the Maxwell model have been developed for studying heat transport phenomena, such as the Maxwell-Eucken model. (Eucken, 1940) and the Maxwell-Garnett model (Garnett and Larmor, 1904), which can account for higher filler concentrations (> 25%) (Pietrak and Wiśniewski, 2015). Another variation of the Maxwell model is the Hamilton-Crosser model (Hamilton and Crosser, 1962), which introduced a shape factor (n) into the expression to account for the shape of the particle inclusions (n = 3 for spherical particles and back to the Maxwell model, and n=6 for the cylindrical particles). Among those variations of the Maxwell model, the Maxwell-Eucken model has been widely used in the literature for determining the ETC of binary mixtures, including porous materials that consist of solid and gas (Maxwell, 1904; Eucken, 1940; Markel, 2016). The Maxwell-Eucken model assumes a dispersion of pores within a continuous matrix of different components, with pores being far enough apart such that the local distortions to the temperature distributions around each of the pores do not interfere with their neighbors' temperature distributions. There are two forms of the Maxwell-Eucken model for a two-component material depending on which component forms the continuous phase (Maxwell, 1904; Jianfeng Wang et al., 2008). The Maxwell-Eucken model can be presented as follows (Maxwell, 1904; Eucken, 1940; Markel, 2016):

$$\kappa_{s+g} = \kappa_g \frac{[(1/2) + p] + (\kappa_s/\kappa_g) (1-p)}{(\kappa_g/2\kappa_s) (1-p) + [1 + (p/2)]}$$
(1)

From Eq. (1), for $\kappa_s \gg \kappa_g$, the term $(\kappa_g/2\kappa_s)(1-p)$ in the denominator can be neglected so that Eq. (1) becomes

$$\kappa_{s+g} \approx \kappa_g \left(\frac{1+2p}{2+p} \right) + \kappa_s \frac{1-p}{1+(p/2)}$$
(2)

where the second term in Eq. (2) represents the solid contribution.

Similarly, Russell (1935) developed a model to calculate the thermal conductivity of porous insulation materials, which is applicable to any system consisting of two phases (solid and gas). This model was derived for porous structures consisting of cubical pores with solid walls of uniform thickness and no struts. This model is also valid for a set of solid cubes surrounded by gas (Russell, 1935; Glicksman, 1994). The upper limit of the solution for the conduction heat transfer was obtained by assuming the conductivity of the solid in the direction lateral to the temperature gradient to be infinite for which the heat flow can be distributed through the top and bottom faces to minimize the resistance and maximize heat flow through the gas and solid wall faces that are in parallel. From this, the overall conductivity due to the gas and solid becomes (Glicksman, 1994)

$$\kappa_{s+g} = \kappa_g \frac{p^{2/3} + (\kappa_s/\kappa_g) \left(1 - p^{2/3}\right)}{(\kappa_g/\kappa_s) \left(p^{2/3} - p\right) + \left(1 - p^{2/3} + p\right)}$$
(3)

where κ_g is the thermal conductivity of the gas, κ_s is solid thermal conductivity, and p is porosity. From Eq. (3), when $\kappa_s \gg \kappa_g$ is the term $(\kappa_g/\kappa_s) \left(p^{2/3}-p\right)$ in the denominator can be neglected so that Eq. (3) becomes

$$\kappa_{s+g} \approx \kappa_g p^{2/3} + \kappa_s \frac{1 - p^{2/3}}{1 - p^{2/3} + p}$$
(4)

The second term in Eq. (4) represents the solid contribution.

For foams with closed cells and struts, Glicksman (1988) proposed a model for determining the contribution of a solid polymer to the ETC; it has been widely used for a variety of polymeric foams. Heat transfer through foams takes place by conduction through solid cell walls and struts, conduction through gas present inside the cell, and the radiation throughout the foam. The total contribution due to solid for foam was derived by the Glicksman model in which the conduction through the solid cell walls and struts are combined, represented by the first and second terms, respectively in Eq. (5) (Glicksman, 1994)

$$\kappa_{es} = \left(\frac{2}{3}\right) \kappa_s \left(1 - p\right) \left(1 - f_s\right) + \left(\frac{1}{3}\right) \kappa_s \left(1 - p\right) f_s \tag{5}$$

$$\frac{\kappa_{es}}{\kappa_s} = \left(\frac{2}{3} - \frac{f_s}{3}\right) (1 - p) \tag{6}$$

where κ_{es} is the contribution to the ETC due to solid conduction and f_s is the fraction of solid in the strut (the walls intersect at cell edges where struts are formed).

Bauer (1993) developed a general analytical approach to study the thermal conductivity of porous media that is suitable over a wide range, from spherical pores to pores of any shape and concentration. It includes an additional parameter, called a shape factor (e) that accounts for the shape of the pore. According to Bauer (1993) for a material with a porous structure, the relationship between the porosity and thermal conductivity can be expressed as follows:

$$\left(\frac{\kappa - \kappa_p}{\kappa_s - \kappa_p}\right) \left(\frac{\kappa_s}{\kappa}\right)^{1 - [2/(3\varepsilon)]} = (1 - p) \tag{7}$$

where κ is the effective thermal conductivity, κ_p is thermal conductivity of pore material, and κ_s is the thermal of the

If the pore is filled with very low thermal conductivity material, $\kappa_p \approx 0$, Eq. (7) becomes

$$\left(\frac{\kappa}{\kappa_s}\right) = (1-p)^{[(3/2)\varepsilon]} \tag{8}$$

Liang and Liu (2009) developed a theoretical model for evaluating the ETC of inorganic particulate polymer composites. Similarly, various models have been proposed to study the heat transfer mechanism in different types of composites and porous insulation materials (Cheng and Vachon, 1970; Nielsen, 1973; Agari et al., 1993; Liang and Li, 2007; Shen and Zhou, 2020; Brooks et al., 2020). Table 1 includes only four EMA models because these models were developed considering the pore geometries, such as cubes and spheres that commonly exist in porous insulation materials. The models were developed for three-dimensional (3D) heat transfer for open- and closed-cell structures, and the results do not depend on the nature of the base material (organic or inorganic).

As mentioned earlier, various EMA models have been developed to determine the impact of porosity on solid conduction. The literature (Fricke et al., 1989; Kuhn et al., 1992; Lu et al., 1995; Sundarram and Li, 2013; Wang et al., 2017) shows that the impacts of porosity on solid conduction in many cases are not well predicted by the EMA models, possibly because of the assumptions made by EMA models (simple pore geometries, regular shapes, and uniform pore sizes) and because they do not account for important factors such as the size effect and interfacial thermal resistance, which could significantly affect heat transfer through insulation materials. Also, for some materials, such as porous

Model	Equations	Refs.	
Russell	$\frac{\kappa_{es}}{\kappa_s} = \frac{1 - p^{2/3}}{1 - p^{2/3} + p}$	Russell (1935b)	
Maxwell-Eucken	$\frac{\kappa_{es}}{\kappa_s} = \frac{1-p}{1+p/2}$	Taxwell (1904), Markel (2016), Eucken (1940)	
Glicksman	$\frac{\kappa_{es}}{\kappa_s} = \left(\frac{2}{3} - \frac{f_s}{3}\right)(1 - p)$	Glicksman (1988)	
Bauer	$\frac{\kappa_{es}}{\kappa_s} = (1 - p)^{1.5\varepsilon}$	Bauer (1993)	

TABLE 1: Equations of various EMA models (3D)

 κ_{es} is contribution to the ETC due to solid conduction,

silica, sound velocity varies significantly with density and can ultimately impact the solid thermal conductivity; this possibility is not accounted for in EMA models (Gross and Fricke, 1992; Bouquerel et al., 2012).

Figure 1 compares the impact of porosity on solid conductivity for various scenarios calculated using EMA models with the values (experimental and simulation results) reported in some literature (for both open- and closed-cell structures). The literature values included conduction and radiation. Thus, we performed additional calculations to extract the impact on solid conductivity. The results show significant differences (2–68%) between the model predicted values and the values from the literature. The results from the models as well as the measurements vary depending on the morphologies of the pores of the materials.

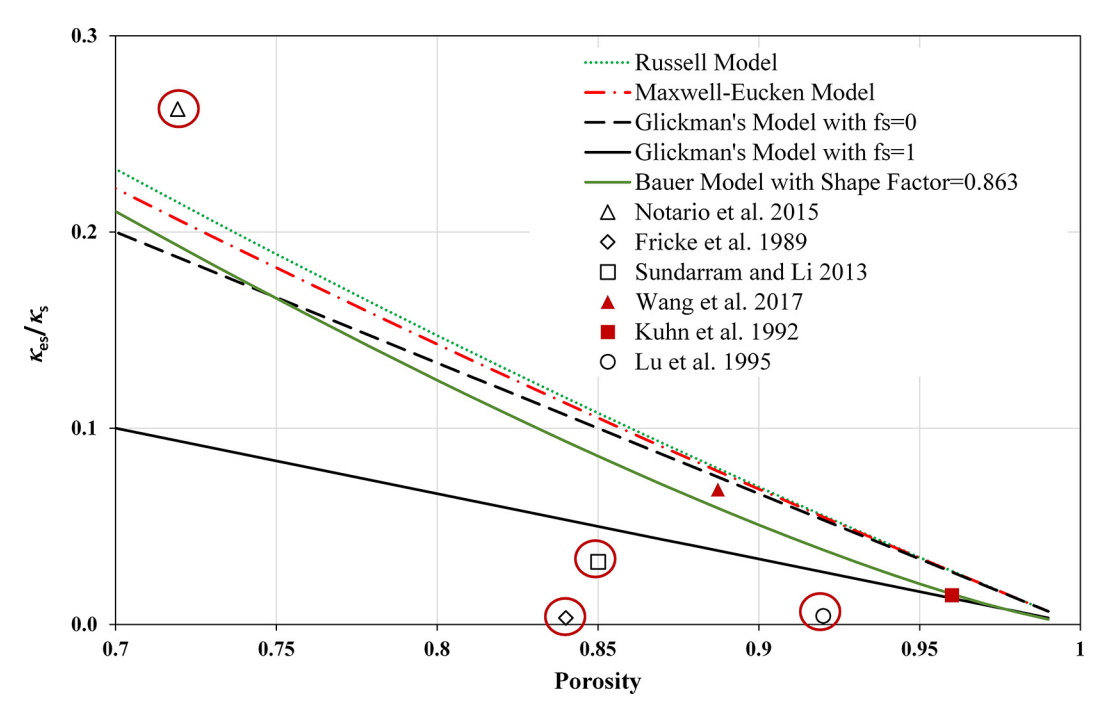


FIG. 1: Comparison of the values predicted by EMA models with the literature values (experimental and simulation results). The symbols that are circled indicate the literature values that are not well captured by the EMA models.

 f_s is the fraction of solid in the strut,

e is shape factor of a randomly oriented pore.

Our hypothesis is that these discrepancies may be due to different morphologies in the cell structure. Thus, in our research, we performed a finite element method (FEM) study, using COMSOL Multiphysics software, for various geometries with different porosities and compared the results to those obtained from the EMA models listed in Table 1. This study will help provide guidance in selecting EMA models for materials with particular pore morphologies. EMA models that use only thermal conductivity and porosity as input parameters might not be able to accurately predict the impacts of porosity on solid conduction for different porous materials. However, if the equation involves an additional fitting parameter, a single equation can provide more accurate predictions for pores of different geometries (Carson et al., 2006). Therefore, EMA models with best-fit values of fitting parameters are also presented based on the FEM results. The rest of this paper is organized as follows: Section 2 describes the details of the simulations via COMSOL Multiphysics for various geometries, and in Section 3, the results obtained from the simulations are compared to those predicted by various EMA models, and improvements in some of the EMA models are presented. The conclusions are presented in Section 4.

2. SIMULATIONS

A 3D numerical framework was developed to calculate the conduction through solids (gas conduction and radiation were neglected) using COMSOL Multiphysics for different types of geometries, such as hollow cube, tightly packed hollow spheres (TPHS), normally stacked hollow spheres (NSHS), and Voronoi structures (see Fig. 2). Porous insulation materials have pores of different geometries; however, we used only selected geometries as representative shapes as they resemble the geometries that were considered in developing the EMA models listed in Table 1. COMSOL itself does not have in-built hollow geometries. Therefore, the following steps were performed to generate hollow spheres in a unit cell. For the TPHS and NSHS, first, a unit cell was generated that had oneeighth of a sphere at each of the eight corners of the cube, half spheres at the center of each of the eight faces, one-quarter of a sphere around each of those half-spheres, and a complete sphere at the center of the cube. Without overlap, the adjacent spheres will have a contact point that can cause difficulty for COMSOL in converging. Therefore, some overlaps (0.2 mm) were introduced between the adjacent spheres for the TPHS and NSHS. Then, an array of unit cells was used for generating porous structures with TPHS and NSHS. For hollow cubes, arrays of identical cubes were used to generate the porous structure. Voronoi tessellations were used for the creation of Voronoi structures, which included the use of Python scripts following the Voro++ developed by Lawrence Berkeley National Laboratory. These structures are commonly used to model the cellular structure of foam materials (Solórzano et al., 2009; Coquard et al., 2012; Vecchio et al., 2016). A Voronoi tessellation is defined by the total area closest to each respective seed point in a multi-point distribution. Voronoi tessellations are used for various applications, such as global atmospheric modeling (Williamson, 1968), studying the structure of void space in twodimensional (2D) and 3D polymer solutions and Yethiraj, 2010), evaluating thermodynamic properties of polycrystalline materials (Li et al., 2012), phase-field simulations of fission gas bubble in nuclear fuels (Li et al., 2013), etc., and it is commonly accepted as being an ideal geometric approximation of an explicitly defined cellular geometry.

The 3D Voronoi geometry was developed from Voro++ (LBL, 2020). The publicly available Pyvoro wrapper was used to run Voro++ in the python environment. A Python code was developed to convert Voro++ coordinate outputs into executable Java methods recognized by COMSOL Multiphysics. These methods allowed for the automated creation of complex Voronoi structures. Different types of Voronoi structures were generated by varying the value of a coefficient, alpha (a), which is applied to the minimum diameter allowed between two Voronoi seed points. At the beginning of a fully ordered body-centric cubic point distribution, a is the ratio allowed for movement of the seed point (0) allowing movement until contact with another seed point and 1 allowing no movement), which does not have an impact on the cell size and wall thickness. As shown in Fig. 2(d), when a = 1, the pore sizes are uniform and they become truncated octahedrons. However, the pores become nonuniform as the value of a decreases [e.g., 0.9 and 0.8, see Figs. 2(e) and 2(f), respectively].

Parametric studies were performed for these geometries to study heat conduction through solids for various porosities. This was done by varying the wall thickness to change the porosity for each type of geometry mentioned above using the Heat Transfer Module of COMSOL Multiphysics. The simulation results were used to calculate the

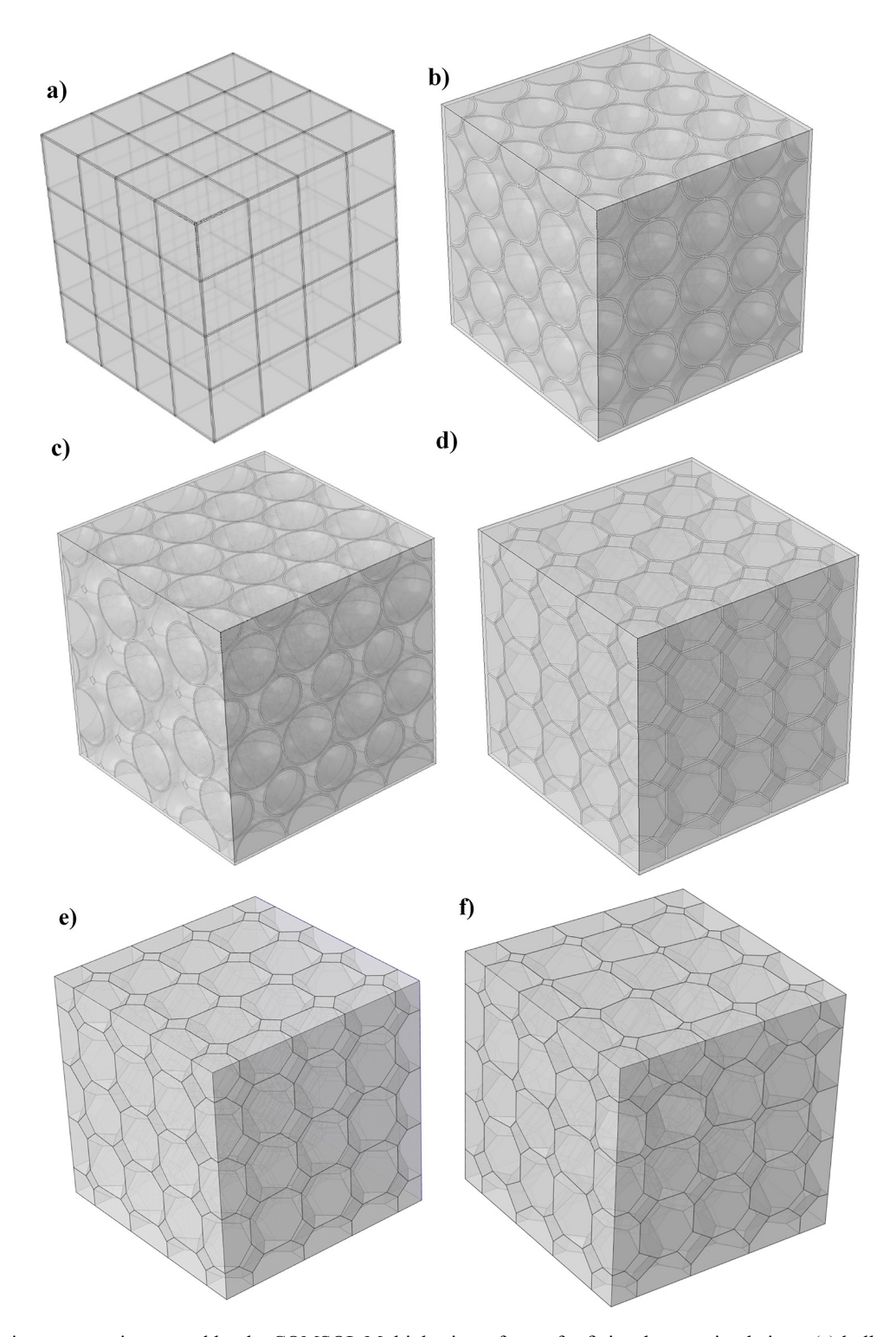


FIG. 2: Various geometries created by the COMSOL Multiphysics software for finite element simulations: (a) hollow cubes, (b) normally stacked hollow spheres, (c) tightly packed hollow spheres, (d) truncated octahedrons (Voronoi structures with a=1), (e) Voronoi structures with a=0.9, and (f) Voronoi structures with a=0.8

contribution of a solid to the ETC and compared to a variety of EMA models to understand how well the simulation results agreed.

To study heat transfer through porous structures, the temperatures of the left (T_L) and right (T_R) faces were held at 350 and 300 K, respectively, along the x-axis; whereas, the other faces were assumed to be adiabatic, as shown in Fig. 3. Only conduction heat transfer through the solid walls was considered in this model. The gaps between the spheres, as well as the interior parts of each type of geometry, were left as is (no materials were defined). To facilitate the specification of boundary conditions, the array of each geometry was enclosed inside a homogeneous cubical shell made up of the same material as the solid walls of each geometry.

The grids of triangular elements were constructed by COMSOL Multiphysics software based on the governing partial differential equation (Laplace's equation) and the specified boundary conditions. Consequently, this constitutes a heat transfer problem, which includes many unknown temperatures. COMSOL Multiphysics implemented a finite element method to determine the temperature at each of these nodes (Chikhi et al., 2013; Floury et al., 2008). The thermal conductivity under a steady state was calculated by

$$\kappa = -\frac{Q}{A} \frac{L}{(T_L - T_R)} \tag{9}$$

where L is the length of the outer cube side, A (= Width $[W] \times$ Height [H]) is the cross-sectional area of each face of the cube, and Q is the total heat flow through each uninsulated face. For heat flow in the x-direction, Q is obtained by

$$Q = \int_{A} -\kappa \frac{\partial T}{\partial x} \partial y \partial z \tag{10}$$

3. RESULTS AND DISCUSSION

Initially, overlaps of 0.2 mm were introduced between the adjacent spheres. An additional study was performed to understand the effect of the amount of overlap upon κ_{es}/κ_s , and the results are shown in Fig. 4. An overlap of 0.2 was considered as the base case. For NSHS, the values of κ_{es}/κ_s changed by as much as \sim 31% for p=0.85, but only \sim 7% for p=0.95, when the overlap was varied from 0.4 to 3.54 mm. However, for TPHS, the values of κ_{es}/κ_s remained within \sim 8%.

The results for different geometries predicted by simulation and those predicted by various EMA models are shown in Fig. 5. For the Bauer model, plots with different e values are presented to show its sensitivity to κ_{es}/κ_s . The value of e was selected as 0.863 for calculations in this work, as it showed an excellent fit with the experimental data from Clark (1948). The value of κ_s can be chosen arbitrarily; we used 0.2 W/(m·K) in all simulations, as it is close to the thermal conductivity of polymers. The pore diameters of each sphere, as well as those of the Voronoi structure

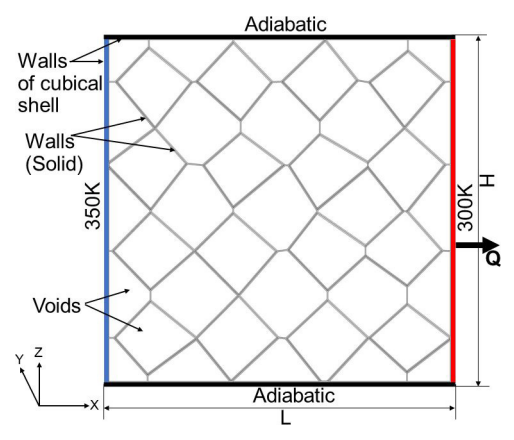


FIG. 3: COMSOL simulation setup with Voronoi structure consisting of random pore sizes with a = 0.8 and p = 0.95

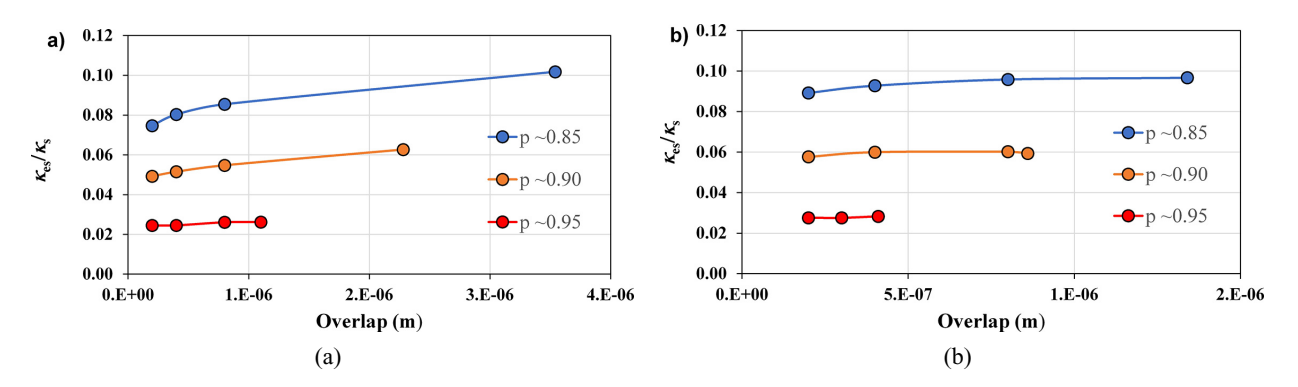


FIG. 4: Impact of overlap between the adjacent spheres on κ_{es} / κ_{s} for different porosities: (a) normally stacked hollow spheres and (b) tightly packed hollow spheres

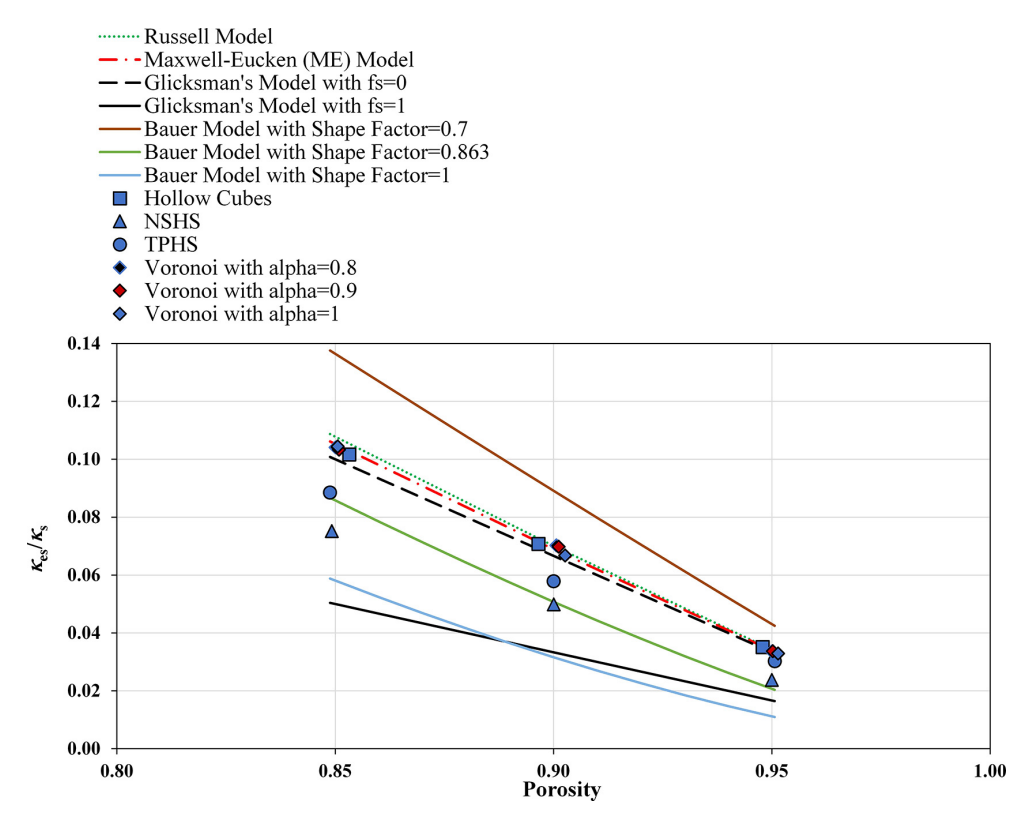


FIG. 5: Comparison of results from simulations with the values predicted by various EMA models

and each side of the hollow cubes, were set as 50, 100, and 200 mm, and the results (κ_{es}/κ_s) were similar for each type of pore morphology. Depending on the pore morphology, the simulation results among the different geometries varied by a factor of up to 1.5. To compare the performances between EMA models and the results from COMSOL simulation, we used a percentage error defined by

$$e_{\text{Model}} = \frac{\left| (\kappa_{\text{es}}/\kappa_{\text{s}})_{\text{Model}} - (\kappa_{\text{es}}/\kappa_{\text{s}})_{\text{Simulation}} \right|}{(\kappa_{\text{es}}/\kappa_{\text{s}})_{\text{Model}}} \times 100\%$$
(11)

where "Model" can be any of the EMA models listed in Table 1.

The comparison of errors from the simulation results with those of the various EMA models is shown in Table 2. As shown in Fig. 5, most of the results from the EMA models match well at higher porosities and start deviating from one another at lower porosities, which can also be observed from the percentage error values shown in Table 2. For the Glicksman model, the value of f_s was set to 0 and 1 to define the upper and lower limits of the model, respectively.

For hollow cubes, the simulation results matched well with the Russell and Maxwell-Eucken models. However, the best prediction was provided by the Maxwell-Eucken model, as its error range was the minimum (0.54–1.20%) compared to other models. Similarly, Voronoi structures with a=1 also showed good agreement with the Maxwell-Eucken model, as indicated by the narrow error range (0.12–0.38%). Results from both structures were a very good match with those of the Maxwell-Eucken model, especially at the highest porosity (0.95). For NSHS and TPHS, the results from simulations were lower than those predicted by most of the EMA models. Although the percentage errors for these geometries were higher, they showed lower percentage errors at the upper limit of the Glicksman model (with $f_s=0$) and of the Bauer model compared to the other EMA models.

Some of the simulation results showed deviations from the results of the EMA models, which can be attributed to the limitations of EMA models. The Maxwell-Eucken model neglects the effect of particle shape and does not consider the mutual interactions among particles (Qian et al., 2017). The percentage errors are higher for hollow spheres than for hollow cubes and Voronoi structures, which can be explained by an analysis of the heat conduction pathways. For hollow cubes and Voronoi structures, there is good contact between the walls of the adjacent particles through which most of the heat flow occurs. However, for hollow spheres, the heat transfer pathways are dependent on the extent of thermal contact between the particles; the shape and packing arrangement of particles can impact the thermal contact between them, leading to higher percentage errors for hollow spheres (Carson et al., 2006).

Some existing EMA models, such as the Bauer and the Glicksman models (these models are described in Section 1), can be further fitted by finding appropriate values of the fitting parameters (e for the Bauer model and f_s for the Glicksman model) included in those models. For this purpose, the results from the Bauer and the Glicksman models were fitted with the COMSOL simulation results obtained for various shapes, as shown in Table 3. For the

TABLE 2: Error from COMSOL simulation results with respect to various EMA models

Shape	Porosity (approx.)	Error for Russell (%)	Error for	Error for	Error for	Error for
			Maxwell-	Glicksman with	Glicksman with	Bauer with
			Eucken (%)	$f_s = 0$ (%)	$f_s = 1 (\%)$	e = 0.863 (%)
Hollow cubes	0.85	3.47	1.20	3.88	107.76	21.85
	0.90	2.55	0.91	2.63	105.25	33.45
	0.95	1.39	0.54	1.22	102.43	61.06
Normally stacked hollow spheres	0.85	30.47	28.80	25.04	49.91	12.69
	0.90	28.81	27.66	25.16	49.67	1.70
	0.95	30.48	29.91	28.72	42.56	14.83
Tightly packed hollow spheres	0.85	18.59	16.63	12.20	75.60	2.10
	0.90	17.38	16.04	13.15	73.70	14.08
	0.95	10.27	9.54	8.03	83.94	48.73
Voronoi with $a = 0.8$	0.85	3.36	1.05	4.16	108.32	21.42
	0.90	0.91	2.53	6.04	112.09	39.56
	0.95	1.50	0.69	0.99	101.98	62.70
Voronoi with $a = 0.9$	0.85	3.58	1.28	3.88	107.76	21.29
	0.90	0.79	2.41	5.90	111.79	39.57
	0.95	0.98	0.17	1.52	103.03	63.75
Voronoi with $a = 1$	0.85	2.70	0.38	4.84	109.67	22.34
	0.90	1.99	0.44	2.90	105.79	36.22
	0.95	0.67	0.12	1.77	103.54	65.37

Model	Shape	Best-Fit Values (e/f_s)		
	Hollow cubes	0.783		
	Normally stacked hollow spheres	0.892		
D	Tightly packed hollow spheres	0.837		
Bauer	Voronoi with $a = 0.8$	0.781		
	Voronoi with $a = 0.9$	0.782		
	Voronoi with $a = 1$	0.783		
	Hollow cubes	0		
Clialannan	Normally stacked hollow spheres	0.507		
Glicksman	Tightly packed hollow spheres	0.245		
	Voronoi with $a = 1$	0		

TABLE 3: Best-fit values of fitting parameters for the Bauer model and the Glicksman model

curve fitting, we did not adjust any parameters in COMSOL modeling. Instead, for each shape, the fitting parameters (ε for the Bauer model and f_s for the Glicksman model) were varied until the errors between the values of κ_{es}/κ_s that were obtained based on the COMSOL simulations results and that obtained from the equations of each model at different porosities reached a minimum value.

Figures 6 and 7 show the plots with the best-fit values of e and of f_s obtained for various geometries. For the Bauer model, the best-fit values of e were between 0.781 and 0.892, and the plots for the hollow cubes and the Voronoi structures with best-fit values seem to be overlapped in Fig. 6. Similarly, the best-fit values of f_s for the Glicksman

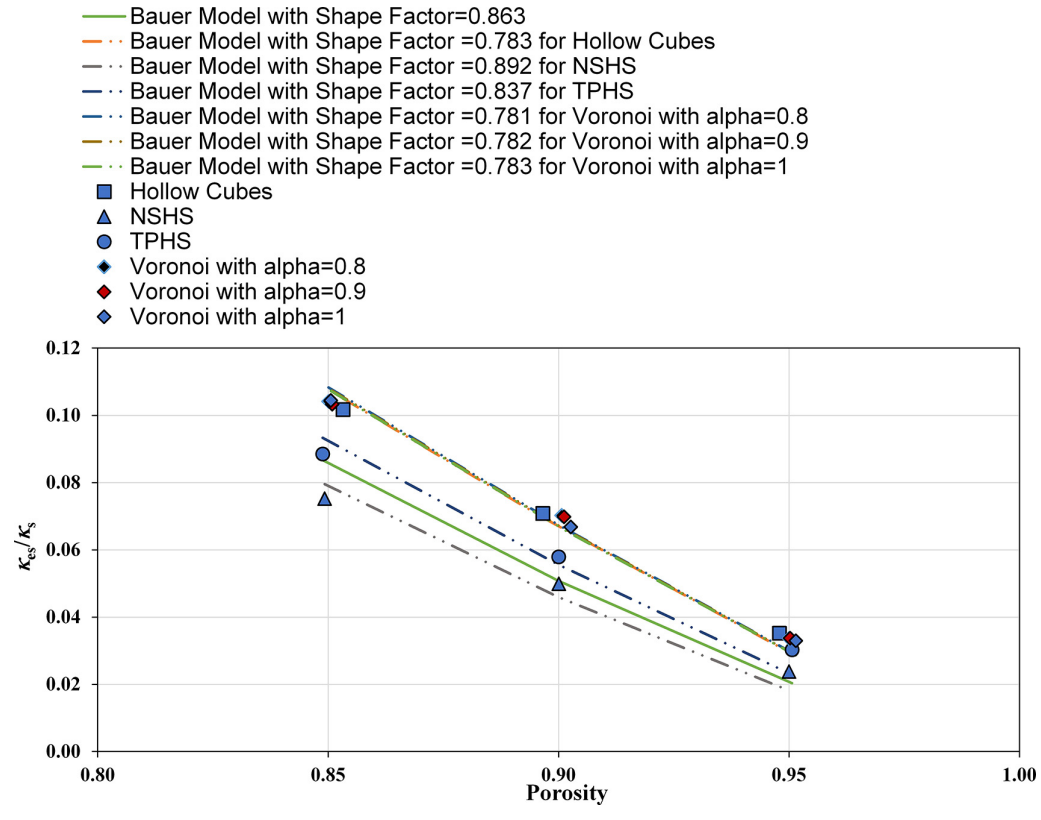


FIG. 6: Bauer model with best fit values of e for various geometries

- · · Glicksman's Model with fs=0
- · · Glicksman's Model with fs =0.245 for TPHS
- Glicksman's Model with fs =0.507 for NSHS
- Hollow Cubes
- NSHS
- TPHS
- ◆ Voronoi with alpha=0.8
- ♦ Voronoi with alpha=0.9
- ♦ Voronoi with alpha=1

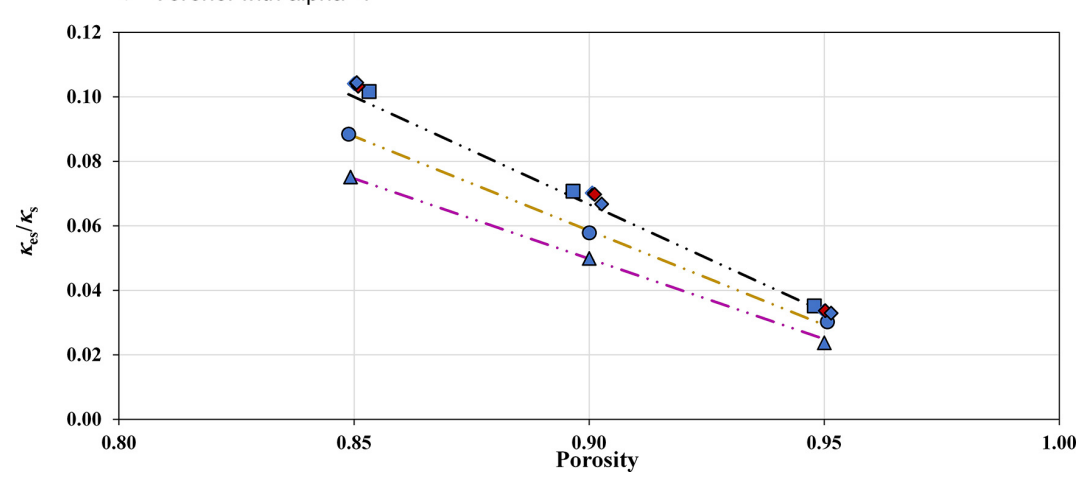


FIG. 7: The Glicksman model with best fit values of f_s for various geometries

model for hollow cubes and Voronoi structures were 0, while for the NSHS and TPHS, the values were 0.507 and 0.245.

4. CONCLUSIONS

In this work, a FEM study was performed using COMSOL Multiphysics for porous insulation materials with various pore morphologies. The results were compared to those obtained from various EMA models to examine how the variations in pore morphology would affect the impact on solid conduction. Three-dimensional heat transfer simulation results showed that hollow cubes and Voronoi structures showed good agreement with the Maxwell-Eucken model compared to other EMA models. However, compared to the EMA models, the results from NSHS and TPHS showed larger errors. By adjusting the Bauer model's geometry fitting parameter and the strut fraction fitting parameter in the Glicksman model, we were able to obtain a good fit for the results from hollow spheres as well. The results of this study will provide guidance for choosing the proper EMA models for given pore morphologies and will have a significant impact on analytical and experimental work on thermal insulation materials.

ACKNOWLEDGMENTS

This work is supported by the project entitled, "Models to Evaluate and Guide the Development of Low Thermal Conductivity Materials for Building Envelopes," funded by the Building Technologies Office, Office of Energy Efficiency and Renewable Energy, of the U.S. Department of Energy.

This paper has been authored by UT-Battelle, LLC, under contract with the U.S. Department of Energy (DOE). The U.S. Government retains and the publisher, by accepting the paper for publication, acknowledges that the U.S. Government retains a nonexclusive, paid-up, irrevocable, worldwide license to publish or reproduce the published form of this paper or allow others to do so, for U.S. Government purposes. DOE will provide public access to these

results of federally sponsored research in accordance with the DOE Public Access Plan (http://energy.gov/downloads/doe-public-access-plan).

REFERENCES

- Agari, Y., Ueda, A., and Nagai, S., Thermal Conductivity of a Polymer Composite, *J. Appl. Polym. Sci.*, vol. **49**, no. 9, pp. 1625–1634, 1993.
- Baetens, R., Jelle, B.P., Thue, J.V., Tenpierik, M.J., Grynning, S., Uvsløkk, S., and Gustavsen, A., Vacuum Insulation Panels for Building Applications: A Review and Beyond, *Energy Build.*, vol. **42**, no. 2, pp. 147–172, 2010.
- Bauer, T.H., A General Analytical Approach toward the Thermal Conductivity of Porous Media, *Int. J. Heat Transf.*, vol. **36**, no. 17, pp. 4181–4191, 1993.
- Bouquerel, M., Duforestel, T., Baillis, D., and Rusaouen, G., Heat Transfer Modeling in Vacuum Insulation Panels Containing Nanoporous Silicas—A Review, *Energy Build.*, vol. **54**, pp. 320–336, 2012.
- Brooks, A.L., Shen, Z., and Zhou, H., Development of a High-Temperature Inorganic Synthetic Foam with Recycled Fly-Ash Cenospheres for Thermal Insulation Brick Manufacturing, *J. Cleaner Prod.*, vol. **246**, p. 118748, 2020.
- Cai, S., Cremaschi, L., and Ghajar, A.J., Pipe Insulation Thermal Conductivity under Dry and Wet Condensing Conditions with Moisture Ingress: A Critical Review, *HVAC&R Res.*, vol. **20**, no. 4, pp. 458–479, 2014.
- Carson, J.K., Lovatt, S.J., Tanner, D.J., and Cleland, A.C., Predicting the Effective Thermal Conductivity of Unfrozen, Porous Foods, *J. Food Eng.*, vol. **75**, no. 3, pp. 297–307, 2006.
- Cheng, S.C. and Vachon, R.I., A Technique for Predicting the Thermal Conductivity of Suspensions, Emulsions and Porous Materials, *Int. J. Heat Mass Transf.*, vol. 13, no. 3, pp. 537–546, 1970.
- Chikhi, M., Agoudjil, B., Haddadi, M., and Boudenne, A., Numerical Modelling of the Effective Thermal Conductivity of Heterogeneous Materials, *J. Thermoplast. Compos. Mat.*, vol. **26**, no. 3, pp. 336–345, 2013.
- Clark, N.O., The Electrical Conductivity of Foam, Trans. Faraday Soc., vol. 44, pp. 13-15, 1948.
- Coquard, R., Randrianalisoa, J., and Baillis, D., Computational Prediction of Radiative Properties of Polymer Closed-Cell Foams with Random Structure, *Int. Symp. Adv. Computational Heat Transf.*, Bath, England, pp. 793–817, 2012.
- Deshmukh, G., Birwal, P., Datir, R., and Patel, S., Thermal Insulation Materials: A Tool for Energy Conservation, *J. Food Process. Tech.*, vol. **8**, no. 4, pp. 1–4, 2017.
- Eucken, A., Allgemeine Gesetzmäßigkeiten Für Das Wärmeleitvermögen Verschiedener Stoffarten Und Aggregatzustände, Forschung Auf Dem Gebiete Des Ingenieurwesens, vol. 11, no. 1, pp. 6–20, 1940.
- Floury, J., Carson, J., and Pham, Q.T., Modelling Thermal Conductivity in Heterogeneous Media with the Finite Element Method, *Food Bioprocess Tech.*, vol. 1, no. 2, pp. 161–170, 2008.
- Fricke, J., Hümmer, E., Morper, H.-J., and Scheuerpflug, P., Thermal Properties of Silica Aerogels, *J. Phys. Colloq.*, vol. 24, no. C4, pp. C4-87–C4-97, 1989.
- Garnett, J.C.M. and Larmor, J., Colours in Metal Glasses and in Metallic Films., Proc. R. Soc. London, vol. 73, pp. 488-496, 1904.
- Glicksman, L.R., Methods to Enhance the Insulating Values of Closed-Cell Foam, Massachusetts Institute of Technology, Cambridge, pp. 149–156, 1988; accessed from https://web.ornl.gov/sci/buildings/conf-archive/1989%20B4%20papers/014.pdf
- Glicksman, L.R., Heat Transfer in Foams, Low Density Cellular Plastics, Springer, Dordrecht, pp. 104–152, 1994.
- Gross, J. and Fricke, J., Ultrasonic Velocity Measurements in Silica, Carbon and Organic Aerogels, *J. Noncryst. Solids*, vol. **145**, no. C, pp. 217–222, 1992.
- Hamilton, R.L. and Crosser, O.K., Thermal Conductivity of Heterogeneous Two-Component Systems, *Ind. Eng. Chem. Fundam.*, vol. 1, no. 3, pp. 187–191, 1962.
- He, Y.-L. and Xie, T., Advances of Thermal Conductivity Models of Nanoscale Silica Aerogel Insulation Material, *Appl. Thermal Eng.*, vol. **81**, pp. 28–50, 2015.
- Hrubesh, L.W. and Pekala, R.W., Thermal Properties of Organic and Inorganic Aerogels, *J. Mater. Res.*, vol. **9**, no. 3, pp. 731–738, 1994.
- Hu, F., Wu, S., and Sun, Y., Hollow-Structured Materials for Thermal Insulation, Adv. Mater., p. 1801001, 2018.

- Jelle, B.P., Gustavsen, A., and Baetens, R., The Path to the High Performance Thermal Building Insulation Materials and Solutions of Tomorrow, *J. Build. Phys.*, vol. **34**, no. 2, pp. 99–123, 2010.
- Kayfeci, M. and Keçebaş, A., Effect of Optimum Insulation Thickness on Refrigeration Costs for Different Climate Zones, *J. Energy Eng.*, vol. **139**, no. 1, pp. 54–59, 2013.
- Kuhn, J., Ebert, H.-P., Arduini-Schuster, M.C., Büttner, D., and Fricke, J., Thermal Transport in Polystyrene and Polyurethane Foam Insulations, *Int. J. Heat Mass Transf.*, vol. **35**, no. 7, pp. 1795–1801, 1992.
- LBL, Voro++—A 3D Voronoi Cell Software Library [Online], Lawrence Berkeley Laboratory; accessed May 16, 2020 from http://math.lbl.gov/voro++/
- Li, D., Li, Y., Hu, S., Sun, X., and Khaleel, M., Predicting Thermal Conductivity Evolution of Polycrystalline Materials under Irradiation Using Multiscale Approach, *Metall. Mater. Trans. A*, vol. **43**, no. 3, pp. 1060–1069, 2012.
- Li, Y., Hu, S., Montgomery, R., Gao, F., and Sun, X., Phase-Field Simulations of Intragranular Fission Gas Bubble Evolution in UO² under Post-Irradiation Thermal Annealing, *Nucl. Instrum. Meth. Phys. Res. B*, vol. **303**, pp. 62–67, 2013.
- Liang, J.Z. and Li, F.H., Simulation of Heat Transfer in Hollow-Glass-Bead-Filled Polypropylene Composites by Finite Element Method, *Polym. Test.*, vol. **26**, no. 3, pp. 419–424, 2007.
- Liang, J.Z. and Liu, G.S., A New Heat Transfer Model of Inorganic Particulate-Filled Polymer Composites, J. Mater. Sci., vol. 44, no. 17, pp. 4715–4720, 2009.
- Lu, X., Caps, R., Fricke, J., Alviso, C.T., and Pekala, R.W., Correlation between Structure and Thermal Conductivity of Organic Aerogels, *J. Noncryst. Solids*, vol. **188**, no. 3, pp. 226–234, 1995.
- Markel, V.A., Introduction to the Maxwell Garnett Approximation: Tutorial, *J. Opt. Soc. Am. A*, vol. 33, no. 7, pp. 1244–1256, 2016.
- Maxwell, J.C., A Treatise on Electricity and Magnetism, Clarendon Press, Oxford, 1904.
- Nielsen, L.E., Thermal Conductivity of Particulate-Filled Polymers, J. Appl. Polym. Sci., vol. 17, no. 12, pp. 3819–3820, 1973.
- Pietrak, K. and Wiśniewski, T., A Review of Models for Effective Thermal Conductivity of Composite Materials, *J. Power Tech.*, vol. **95**, no. 1, pp. 14–24, 2015.
- Qian, L., Pang, X., Zhou, J., Yang, J., Lin, S., and Hui, D., Theoretical Model and Finite Element Simulation on the Effective Thermal Conductivity of Particulate Composite Materials, *Composites: B*, vol. **116**, pp. 291–297, 2017.
- Reimi, C., Dominique, B., and Daniel, Q., Radiative Properties of Expanded Polystyrene Foams, *J. Heat Transf.*, vol. 131, no. 1, p. 012702, 2009.
- Russell, H.W., Principles of Heat Flow in Porous Insulators, J. Am. Ceram. Soc., vol. 18, nos. 1-12, pp. 1-5, 1935.
- Shen, Z. and Zhou, H., Predicting Effective Thermal and Elastic Properties of Cementitious Composites Containing Polydispersed Hollow and Core-Shell Micro-Particles, *Cement Concrete Compos.*, vol. **105**, p. 103439, 2020.
- Shrestha, S.S., Rai, A., Feng, T., Zhang, M., Hun, D.E., Biswas, K., and Desjarlais, A.O., Review of Models to Evaluate and Guide the Development of Low-Thermal-Conductivity Materials, *Buildings XIV Int. Conf.*, pp. 67–80, 2019.
- Solórzano, E., Rodriguez-Perez, M.A., Lázaro, J., and de Saja, J.A., Influence of Solid Phase Conductivity and Cellular Structure on the Heat Transfer Mechanisms of Cellular Materials: Diverse Case Studies, *Adv. Eng. Mater.*, vol. **11**, no. 10, pp. 818–824, 2009
- Sundarram, S.S. and Li, W., On Thermal Conductivity of Micro- and Nanocellular Polymer Foams, *Polym. Eng. Sci.*, vol. **53**, no. 9, pp. 1901–1909, 2013.
- Sung, B.J. and Yethiraj, A., Structure of Void Space in Polymer Solutions, Phys. Rev. E, vol. 81, no. 3, p. 031801, 2010.
- Vecchio, I., Redenbach, C., Schladitz, K., and Kraynik, A.M., Improved Models of Solid Foams Based on Soap Froth, *Comput. Mater. Sci.*, vol. **120**, pp. 60–69, 2016.
- Walser, R., Metamaterials: An Introduction, Introduction to Complex Mediums for Optics and Electromagnetics, Bellingham, WA: SPIE, pp. 295–316, 2009.
- Wang, G., Zhao, J., Mark, L.H., Wang, G., Yu, K., Wang, C., Park, C.B., and Zhao, G., Ultra-Tough and Super Thermal-Insulation Nanocellular PMMA/TPU, *Chem. Eng. J.*, vol. **325**, pp. 632–646, 2017.
- Wang, J., Carson, J.K., North, M.F., and Cleland, D.J., A New Structural Model of Effective Thermal Conductivity for Heterogeneous Materials with Co-Continuous Phases, *Int. J. Heat Mass Transf.*, vol. **51**, nos. 9-10, pp. 2389–2397, 2008.

Wang, M. and Pan, N., Predictions of Effective Physical Properties of Complex Multiphase Materials, *Mater. Sci. Eng. R*, vol. **63**, no. 1, pp. 1–30, 2008.

Williamson, D.L., Integration of the Barotropic Vorticity Equation on a Spherical Geodesic Grid, *Tellus*, vol. **20**, no. 4, pp. 642–653, 1968